GSA DATA REPOSITORY 2011230

Molybdenum isotopic records across the Precambrian-Cambrian boundary

Hanjie Wen[1] Jean Carignan[2*] Yuxu Zhang[1] Haifeng Fan[1] Christophe Cloquet[2] Shirong Liu[1]

[1]*State Key Laboratory of Ore Deposit Geochemistry (SKLODG), Institute of Geochemistry, Chinese Academy of Sciences, Guiyang, 550002 , China ;*

[2] *Centre de Recherches Pétrographiques et Géochimiques (CRPG), Nancy-Université, CNRS/INSU, 15 rue Notre-Dame-des-Pauvres B.P. 20 F-54501 Vandœuvre lès Nancy, France*

**now at : TAKUVIK: International Center for Arctic and sub-Arctic eco-geosystems studies, CNRS UMI 3376, Université Laval, Centre d'études nordiques, local 1202, Pavillon Abitibi-Price, 2405 rue de la Terrasse, Québec, Qc, G1V 0A6, Canada*

Section 1. Chemistry and mass spectrometry

Samples were collected from the Meishucun and Gezhongwu sections as described in the text. A total of 44 samples were analyzed for major and trace elements and Mo isotopes. Prior to geochemical analyses, the weathered surface was removed from each sample, and cleaned with distilled water and dried. Then the samples were crushed to a mesh size of -200. Chemical analyses were performed using different methods. Major and trace elements were analyzed by XRF (Axios, PW4400) and ICP-MS (PE Elan DR-e), respectively, at the State Key Lab of Ore Deposit Geochemistry (SKLODG), Institute of Geochemistry of the Chinese Academy of Sciences. The analytical uncertainty for elemental concentrations was generally better than 5%. Total organic C and total S contents in the samples were measured by a C-S element analytical instrument (CS-314) in the analytical center of the Institute of Geochemistry, Chinese Academy of Sciences. Fe species were measured by a sequential extraction procedure described previously by Poulton and Canfield (2005).

After determining Mo concentrations, sample powders with an equivalent of >100 ng Mo were oxidized at 600°C for about 8 h, and then transferred to a Teflon beaker. Samples were digested using a mixture of HF and HNO_3 (1:2) at 100°C for at least 16 h until the samples were completely dissolved. An improved anion/cation exchange resin double-column procedure was used to separate Mo from natural samples, as described by Zhang et al. (2009). This method can yield a recovery of Mo of 97.49%±0.27%. The potential interferences on Mo isotopes, including Zr, Fe, Mn and other interfering matrix elements

were present at negligible levels relative to Mo, and with lower volumes of Mo elution solution than previously reported (Pietruszka 2006).

The Mo isotopic measurements were performed at the Centre de Recherches Pétrographiques et Géochimiques (CRPG, France) using an Isoprobe MC-ICP-MS. Samples were introduced using a cyclonic chamber system with a PFA pneumatic nebulizer in free aspiration mode. All samples and bracketing reference solutions were run in 2 blocks of 15 cycles of measurements on each amu. This system typically generated a total Mo signal of about 57 V/ppm, at an uptake rate of about 100 µl/min, which corresponds to ca. 75 ng Mo analyzed. After each run, the nebulizer and spray chamber were rinsed with 0.6 M HNO_3 until the signal intensity reached the original background level (generally after 3 min).

Signal acquisition was performed according to the following collector configurations. $^{91}Zr^+$, $^{92}Mo^+$, $^{94}Mo^+$, $^{95}Mo^+$, $^{96}Mo^+$, $^{97}Mo^+$, $^{98}Mo^+$, $^{99}Ru^+$, and $^{100}Mo^+$ ion beams were collected by Faraday cups at Low 3, Low 2, Central, High 1, High 2, High 3, High 4, High 5 and High 6 positions, respectively. The Standard-Sample Bracketing (SSB) method was used to calculate delta values, as reported for Fe and Cu (Zhu et al. 2000; Rouxel et al. 2002), and for Se (Carignan and Wen 2007). Concentrations of samples and reference Mo samples (bracketing Mo reference: JMC) were matched to within 10%. Analyses were conducted in the static mode. The signal of a blank solution was subtracted for all measured masses. Instrumental drift was corrected by averaging the measured ratios of the bracketing reference solution. Only sections presenting linear or smooth drifts for the measured reference solution were considered and used for calculating sample delta values. A JMC Mo solution (lot#13989C) was used as an internal reference standard. For the presentation of results, δ-notation was utilized, as defined by the relationship:

$$\delta^{x}Mo(‰)=[(^{x}Mo/^{95}Mo)_{sample}/(^{x}Mo/^{95}Mo)_{std} -1]\times 1000 ‰$$

Where x is the ^{92}Mo, ^{94}Mo, ^{96}Mo, ^{97}Mo, ^{98}Mo or ^{100}Mo isotope.

Repeated measurements of pure Mo solutions yielded reproducibility of better than ca. ±0.0.08‰ (2σ) on the $\delta^{97}Mo$ value. Repeat analyses of artificially fractionated Mo solutions through chemistry yielded a mean $\delta^{97/95}Mo$ composition of 1.05 ± 0.09 ‰ (2sd, n=19), which is consistent with the reported values (Wen et al., 2010). Analyses of granite standard GSR-1 gave a mean $\delta^{97/95}Mo$ composition of -0.21± 0.0.7 ‰ (2 sd, n=12); and repeat measurements of an organic-rich sediments (GSD-3, 92 ppm Mo) yielded the mean $\delta^{97/95}Mo$ value of 0.70 + 0.06 ‰ (2 sd, n=8). We analyzed in duplicate and triplicate some samples and found an overall reproducibility better than ±5% for [Mo] between preparations and about ±0.15‰ (0.1 - 0.2) for delta values.

Table DR1 Chemical composition of samples across the Precambrian-Cambrian boundary from the Meishucun and Gezhongwu sections from Guizhou, Southern China.

Sample	location	description	Mo	TOC	Total S	SiO_2	Fe_2O_3	MnO	Al_2O_3	TiO_2	CaO	MgO	P_2O_5
			ppm	%	%	%	%	%	%	%	%	%	%
Meishucun section													
BYS-02	BYS	dolomite	12.70	0.02	0.05	15.99	0.68	0.07	1.93	0.11	25.46	16.56	1.51
BYS-0	BYS	dolomite	1.65	0.06	0.08	30.59	1.54	0.04	7.7	0.45	21.67	7.45	8.79
XWT-03	XWTS	dolomite	0.79	0.02	0.03	6.73	0.47	0.09	0.84	0.06	29.86	18.78	2.76
XWT-10	XWTS	dolomite	1.29	0.02	0.04	6.80	0.38	0.12	0.65	0.03	28.92	18.59	2.82
XWT-11	XWTS	dolomite	0.88	0.03	0.13	5.02	0.41	0.12	0.54	0.03	31.42	18.16	4.54
XWT-12	XWTS	dolomite	0.76	0.01	0.04	9.44	0.46	0.09	0.75	0.01	29.97	16.07	4.37
XWT-14	XWTS	dolomite	1.43	0.03	0.10	21.87	0.64	0.11	2.03	0.13	23.73	14.33	3.22
XWT-15	XWTS	dolomite	1.22	0.04	0.25	5.82	0.74	0.12	0.62	0.03	31.97	16.42	7.09
ZYC1	ZYC	phosphorite	1.00	0.19	0.07	2.18	0.20	0.02	0.21	<0.01	52.08	1.88	36.22
ZYC2	ZYC	phosphorite	1.19	0.11	0.05	4.56	0.16	0.03	0.16	<0.01	49.49	2.85	33.51
ZYC4	ZYC	phosphorite	2.16	0.23	0.02	5.62	0.33	0.03	0.26	0.04	48.02	2.94	32.38
ZYC7	ZYC	phosphorite	1.32	0.17	0.02	10.11	0.32	0.05	0.35	0.03	41.28	6.63	23.23
ZYC8	ZYC	phosphorite	1.45	0.15	0.05	11.32	0.31	0.05	0.42	0.01	41.31	6.11	23.80
ZYC11	ZYC	phosphorite	2.59	0.03	0.05	2.45	0.38	0.02	0.15	<0.01	50.94	1.92	35.48
ZYC13	ZYC	phosphorite	2.19	0.09	0.04	2.04	0.20	0.02	0.16	<0.01	51.67	1.68	36.26
ZYC15	ZYC	phosphorite	6.15	0.01	0.06	49.96	0.51	0.01	0.11	<0.01	27.26	0.11	18.71
ZYC17	ZYC	phosphorite	1.29	0.12	0.03	8.21	0.39	0.02	0.43	0.01	46.37	3.48	30.02
ZYC20	ZYC	phosphorite	0.94	0.08	0.05	4.01	0.66	0.08	0.33	<0.01	38.54	11.60	16.02
ZYC21	ZYC	phosphorite	2.15	0.16	0.04	3.19	0.29	0.02	0.19	<0.01	48.55	3.79	32.54
ZYC22	ZYC	phosphorite	1.28	0.13	0.01	4.11	0.43	0.06	0.34	0.02	45.97	5.83	27.76
ZYC24	ZYC	phosphorite	1.23	0.07	0.03	3.79	0.56	0.14	0.31	0.01	36.70	13.86	12.28
ZYC27	ZYC	phosphorite	2.03	0.03	0.05	24.95	1.31	0.14	2.96	0.23	23.84	12.28	4.60
DH-03	DH	dolomite	0.83	0.01	0.03	1.75	0.45	0.08	0.06	<0.01	29.36	20.21	0.20
DH-04	DH	dolomite	0.95	0.01	0.03	1.75	0.50	0.08	0.08	<0.01	30.13	19.90	0.24
K-B-02	SYT	Bentonite	2.19	0.05	0.04	49.71	4.21	0.07	15.65	0.44	8.54	1.94	5.99
9—4	SYT	siltstone	7.03	1.53	1.43	63.14	2.37	0.03	12.73	0.65	2.90	2.98	0.46
9—14	SYT	siltstone	9.05	1.43	1.03	58.40	3.05	0.05	11.11	0.59	5.34	4.56	0.50
9—19	SYT	siltstone	8.78	1.25	1.04	59.84	3.10	0.04	12.44	0.65	3.54	4.11	0.39
9—29	SYT	siltstone	5.77	1.39	1.68	60.84	3.88	0.04	13.89	0.74	2.20	3.91	0.31
9—34	SYT	siltstone	6.95	1.34	1.56	58.06	4.08	0.05	13.19	0.73	3.02	4.58	0.32
9—39	SYT	siltstone	6.07	1.76	0.52	57.38	5.22	0.05	11.87	0.70	3.81	4.75	0.28
9—44	SYT	siltstone	5.76	0.99	1.15	53.40	3.88	0.06	12.14	0.66	5.69	6.05	0.38
9—46	SYT	siltstone	14.40	1.13	1.52	57.03	4.00	0.05	13.2	0.72	3.48	4.84	0.40
9—51	SYT	siltstone	3.79	0.98	2.03	54.11	3.75	0.06	11.66	0.62	5.90	6.15	0.34
9—56	SYT	siltstone	5.93	1.10	2.01	58.03	4.18	0.05	13.47	0.74	3.07	5.01	0.28
9—60	SYT	siltstone	4.63	0.98	1.43	56.68	4.15	0.05	13.41	0.74	3.49	5.35	0.29
9—63	SYT	siltstone	6.73	1.07	1.71	57.42	4.38	0.05	13.33	0.75	3.16	5.22	0.34
9--65	SYT	siltstone	6.08	1.05	1.57	57.50	4.35	0.04	13.52	0.74	3.20	5.19	0.39

Gezhongwu Setion													
JPD-01	DY	dolomite	2.61	0.01		2.54	0.44	0.36	2.83	0.07	28.03	24.69	0.04
GZW-02-18	GZW	phosphorite	2.28	0.10	0.12	5.22	0.60	0.07	0.32	0.05	58.35	0.31	30.70
GZW-02-20	GZW	phosphorite	2.06	0.01	0.18	6.98	0.42	0.05	0.19	0.05	56.32	0.86	30.50
GZW-02-24	GZW	phosphorite	6.41	0.08	0.20	36.10	4.52	0.42	1.75	0.15	32.96	0.61	19.20
GZW-02-32	GZW	phosphorite	6.20	0.09	0.34	25.00	2.76	0.03	0.72	0.10	42.50	1.01	23.90

BYS: Pre-Cambiran Baiyanshao Member; XWTS: Xiaowantoushan Member; ZYC: Zhongyicun Member; DH: Dahai Member; SYT: Shiyantou Member; DY: Pre-Cambrian Dengying Formation

Table DR2 Fe species and isotopic composition of samples across the Precambrian-Cambrian boundary from the Meishucun and Gezhongwu sections, Southern China.

Sample	Location	Description	$\delta^{97/95}$Mo (2σ) (‰)	$\delta^{97/95}$Mo corr. Al (‰)	$\delta^{97/95}$Mo corr. Ti (‰)	Total Fe (%)	Fe_{Py} (%)	Fe_{HR} (%)
Meishucun section								
BYS-02	BYS	dolomite	0.9 ± 0.06	0.91	0.91	0.47	0.001	0.42
BYS-0	BYS	dolomite	0.7 ± 0.08	1.05	1.32	1.08	0.001	0.85
XWT-03	XWTS	dolomite	-0.15 ± 0.03	-0.16	-0.17	0.33	0.001	0.27
XWT-10	XWTS	dolomite	-0.25 ± 0.11	-0.26	-0.26	0.27	0.001	0.25
XWT-11	XWTS	dolomite	-0.29 ± 0.09	-0.30	-0.31	0.29	0.001	0.25
XWT-12	XWTS	dolomite	-0.44 ± 0.07	-0.47	-0.45	0.32	0.001	0.26
XWT-14	XWTS	dolomite	-0.34 ± 0.08	-0.38	-0.40	0.45	0.001	0.40
XWT-15	XWTS	dolomite	-0.53 ± 0.11	-0.55	-0.55	0.52	0.001	0.34
ZYC1	ZYC	phosphorite	0.29 ± 0.10	0.29	0.30	0.14	0.006	0.12
ZYC2	ZYC	phosphorite	0.19 ± 0.06	0.19	0.19	0.11	0.004	0.10
ZYC4	ZYC	phosphorite	-0.39 ± 0.08	-0.39	-0.40	0.23	0.004	0.19
ZYC7	ZYC	phosphorite	-0.21 ± 0.11	-0.21	-0.22	0.22	0.005	0.19
ZYC8	ZYC	phosphorite	-0.16 ± 0.03	-0.16	-0.16	0.22	0.002	0.19
ZYC11	ZYC	phosphorite	-0.15 ± 0.06	-0.15	-0.15	0.27	0.009	0.17
ZYC13	ZYC	phosphorite	-0.04 ± 0.07	-0.04	-0.04	0.14	0.010	0.12
ZYC15	ZYC	phosphorite	-0.49 ± 0.13	-0.49	-0.49	0.36	0.002	0.35
ZYC17	ZYC	phosphorite	1.40 ± 0.04	1.43	1.42	0.27	0.001	0.21
ZYC20	ZYC	phosphorite	1.35 ± 0.05	1.38	1.38	0.46	0.001	0.31
ZYC21	ZYC	phosphorite	1.12 ± 0.09	1.13	1.13	0.20	0.002	0.15
ZYC22	ZYC	phosphorite	1.09 ± 0.10	1.11	1.12	0.30	0.004	0.21
ZYC24	ZYC	phosphorite	1.36 ± 0.12	1.38	1.38	0.39	0.001	0.26
ZYC27	ZYC	phosphorite	0.89 ± 0.08	0.99	1.11	0.92	0.000	0.00
DH-03	DH	dolomite	1.31 ± 0.04	1.32	1.34	0.32	0.000	0.00
DH-04	DH	dolomite	1.36 ± 0.07	1.37	1.39	0.35	0.000	0.00
K-B-02	SYT	Bentonite	1.4 ± 0.16	1.40	1.40	2.95	0.000	0.00
9—4	SYT	siltstone	0.51 ± 0.08	0.59	0.61			
9—14	SYT	siltstone	-0.19 ± 0.11	-0.21	-0.21			
9—19	SYT	siltstone	-0.01 ± 0.08	-0.01	-0.01			
9—29	SYT	siltstone	0.19 ± 0.07	0.23	0.24			
9—34	SYT	siltstone	-0.05 ± 0.09	-0.06	-0.06			
9—39	SYT	siltstone	0.01 ± 0.04	0.01	0.01			
9—44	SYT	siltstone	0.02 ± 0.06	0.02	0.02			
9—46	SYT	siltstone	0.04 ± 0.08	0.04	0.04			
9—51	SYT	siltstone	0.3 ± 0.10	0.38	0.42			
9—56	SYT	siltstone	0.07 ± 0.07	0.08	0.09			
9—60	SYT	siltstone	0.59 ± 0.12	0.74	0.81			
9—63	SYT	siltstone	0.55 ± 0.11	0.64	0.68			
9--65	SYT	siltstone	0.32 ± 0.08	0.38	0.40			

Gezhongwu Setion					
JPD-01	DY	dolomite	0.69 ± 0.11	0.75	0.72
GZW-02-18	GZW	phosphorite	-0.22 ± 0.08	-0.22	-0.23
GZW-02-20	GZW	phosphorite	-0.45 ± 0.06	-0.45	-0.47
GZW-02-24	GZW	phosphorite	-0.31 ± 0.05	-0.32	-0.32
GZW-02-32	GZW	phosphorite	1.4 ± 0.09	1.41	1.44

Note: The corrected isotopic composition was calculated following the formula: $\delta^{97/95}Mo_{auth}= [(\delta^{97/95}Mo_{tot}\cdot Mo_{tot}- \delta^{97/95}Mo_{det}\cdot Mo_{det})/Mo_{auth}]$, in which the detrital Mo concentration (Mo_{det}) was then given by $Mo_{det}=[(Mo/X)crust\cdot X_{tot}]$, where X = Al or Ti, and the authigenic Mo concentration was $Mo_{auth}=[Mo_{tot}-Mo_{det}]$. We applied a detritus correction assuming Mo concentration of 1.1 ppm, upper crustal Al_2O_3 and TiO_2 concentrations of 15.4 wt.% and 0.64 wt.%, respectively (all values from Rudnick and Gao, 2004), and Mo isotopic composition of 0.0‰, as proposed by Voegelin et al. (2009). Because TiO2 concentrations of TiO_2 for some samples were lower than the determination limit (0.01%), we did calculations using TiO_2=0.01%. Fe_{Py}: Pyrite iron; Fe_{HR}: Highly Reactive iron; Fe species were measured by a simplified sequential extraction procedure described previously by Poulton and Canfield (2005). Here we use HCl-extractable Fe as representing the Fe_{HR} (Highly Reactive Iron). Fe from detrital material (including clay minerals) is very low (See Al and Ti contents) as well as Fe_{py} so that iron derived from these species is negligible compared with other iron fractions extracted from samples. HCl-extractable Fe originates from (oxyhydr)oxides such as ferrihydrite, lepidocrocite, goethite and hematite, and partly from sheet silicates.

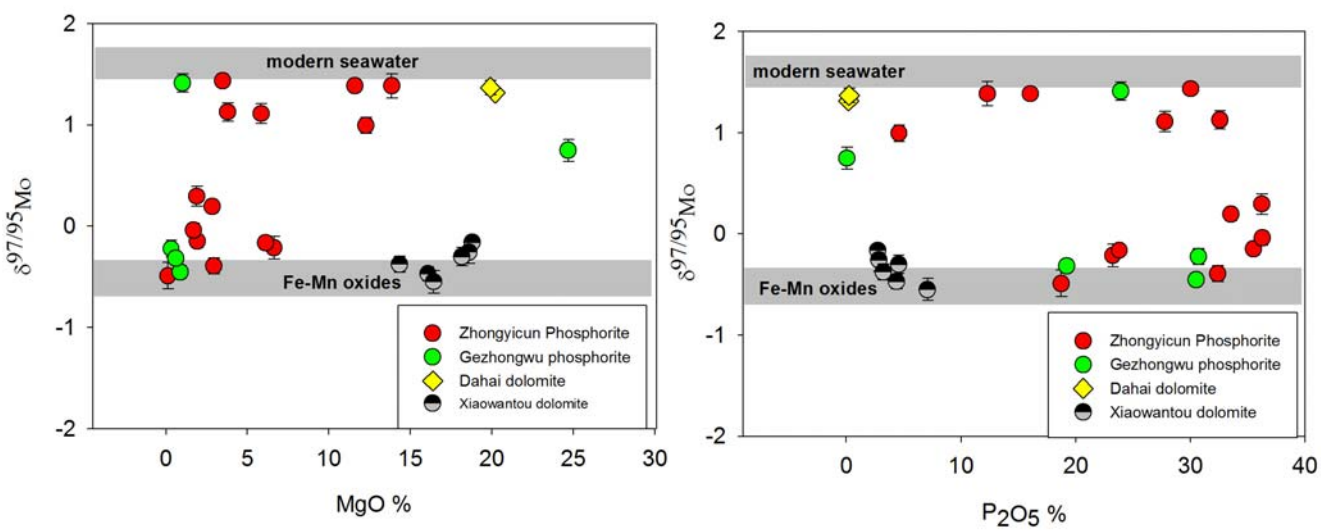

Figure DR1. Correlation between Mo isotopic compositions and MgO and P_2O_5 concentrations in samples from the Meishucun and Gezhongwu sections.

Section 2. Geological setting and stratigraphy

The Ediacaran to early Cambrian successions were well preserved over the Yangtze platform in South China with different paleo-environmental settings, including platform facies, transition belt and protected basin as illustrated in Figure DR 2(Steiner et al., 2001; Guo et al., 2007). In several areas, they are exposed across a transection from platform to basin, offering an opportunity to investigate the stratigraphic features during this critical interval of the Earth history, which can provide clues of sea-level

fluctuations, ocean anoxia, metal accumulation and corresponding ocean-atmosphere-biology evolution.

Two sections are selected for this study, Meishucun section and Gezhongwu section, separated each other by a distance of approximately 400 km (Figure DR2). Paleogeographically, the two sections are located within the carbonate platform, shelf of southern Yangtze platform, which reflects shallow water sedimentation.

Three biostratigraphic markers are found within the Yuhucun Formation. Marker A marks the first appearance of small shelly fossils, while marker B is related to a significant increase in shell diversity and was previously proposed as the Precambrian-Cambrian boundary GSSP. Marker C delineates an important sedimentary transition from evaporitic dolomite facies to organic rich siltstones, which indicate a shift to a deeper basinal environment (Shields and Stille, 2001). A tuff layer (unit 5) separates the Zhongyicun member into two beds - the "upper phrosphorite bed" (units 6 and 7) and the "lower phosphorite bed" (units 3 and 4). Two new U-Pb zircon ages from this tuff layer have been obtained, which date this horizon to 536.5 ± 2.5Ma (LA-ICPMS, Sawaki et al., 2008) and 535.2 ± 1.7Ma (SIMS, Zhu et al., 2009). Both studies of these tuff-derived zircons proposed that marker A is a better candidate for the PC/C boundary than marker B. Considering a PC/C boundary at 540 Ma, markers A and B are separated by ca. 5 Ma. If sedimentary rate is consistent, then sedimentation duration for whole section from unit 1 to unit 8 is about 10Ma.

At the Gezhongwu section, two isochron ages have been obtained, 541±12 Ma (Rb-Sr) and 542±23 Ma (Sm-Nd) for the basal phosphorite, which is equivalent to the Ediacaran-Cambrian boundary proposed by Gradstein et al. (2004). For Gezhongwu section, the sedimentation duration is about 10 Ma, when combined with data from Jiang et al. (2009) for the whole section.

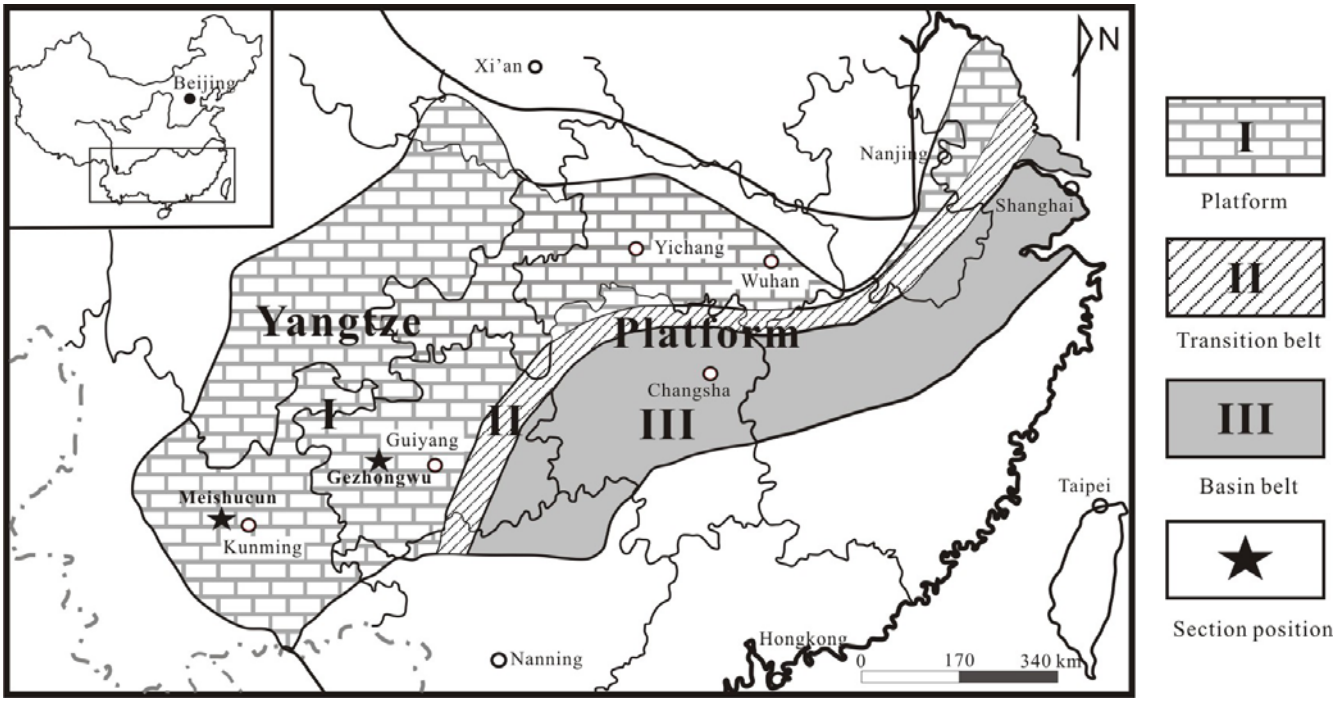

Figure DR2 . Loction of selected sections and stratigraphy, after (Steiner et al., 2001; Guo et al., 2003).

Section 3. Supplemental EPMA observations of phosphorites and associated rocks

Twenty phosphorite samples were observed in thin section with an EPMA-1600 Electron Probe Microanalyzer (EMPA), to examine the surface texture of different types of phosphatic grains. Typical phosphatic grains representing different grain types were mapped for major elements (SiO_2, Al_2O_3, FeO, MnO, MgO, CaO, K_2O, Na_2O, SO_3, P_2O_5, and F) to examine compositional variations within grains.

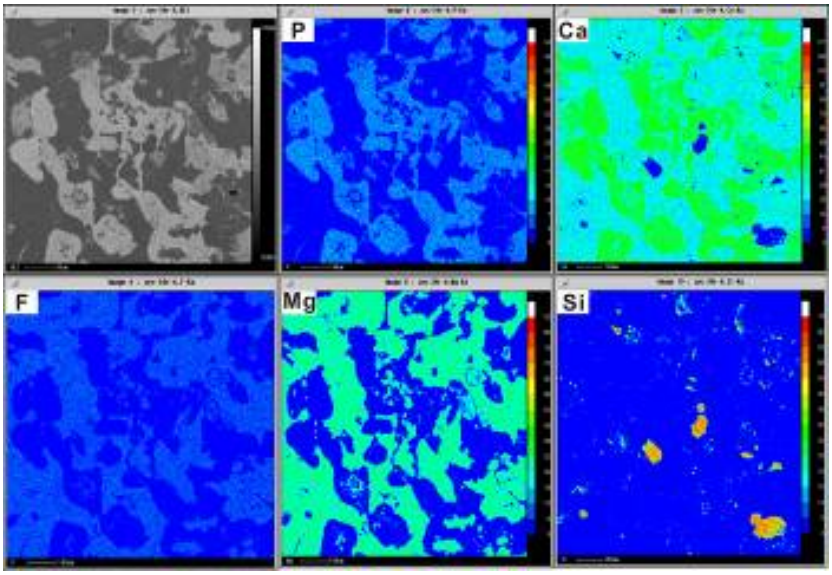

Figure DR3. Elemental mapping of thin sections from typical "pristine" phosphorites in the upper phosphorite bed of the Meishucun section.

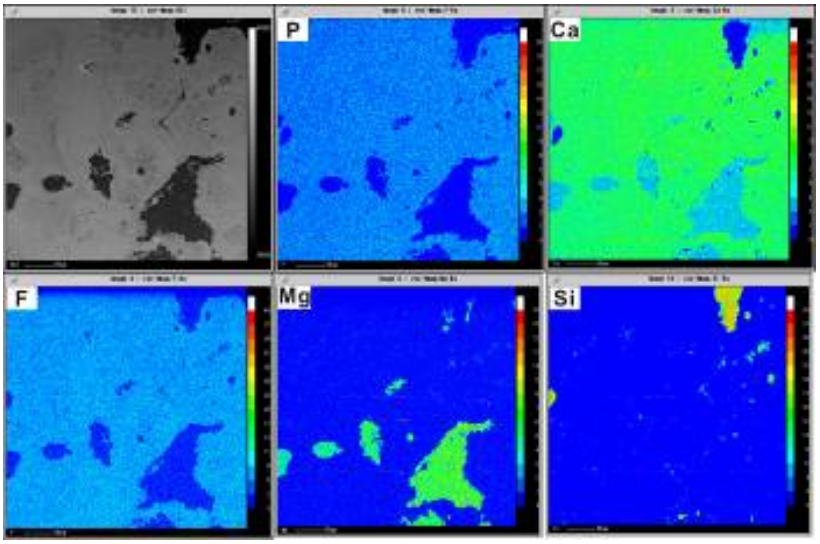

Figure DR4. Elemental mapping of thin sections from typical coated phosphatic grains (reworked phosphorite) in the lower phosphorite bed of the Meishucun section.

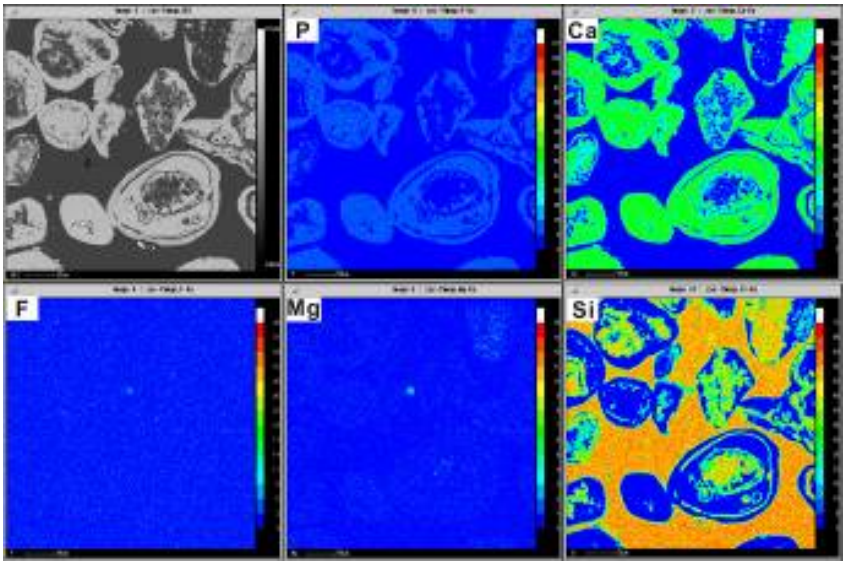

Figure DR5. Elemental mapping of thin section from typical phosphatic intraclasts (reworked phosphorite) in the lower phosphorite bed of the Meishucun section.

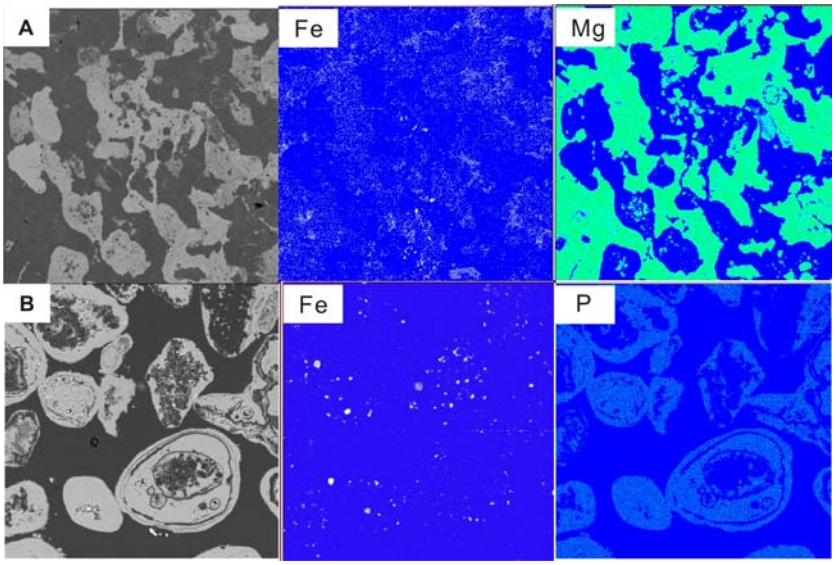

Figure DR6. Relationship of Fe, Mg, and P, based on elemental mapping of thin sections from typical "pristine" (A) and reworked phosphorites (B) in the upper and lower phosphorite bed of the Meishucun section.

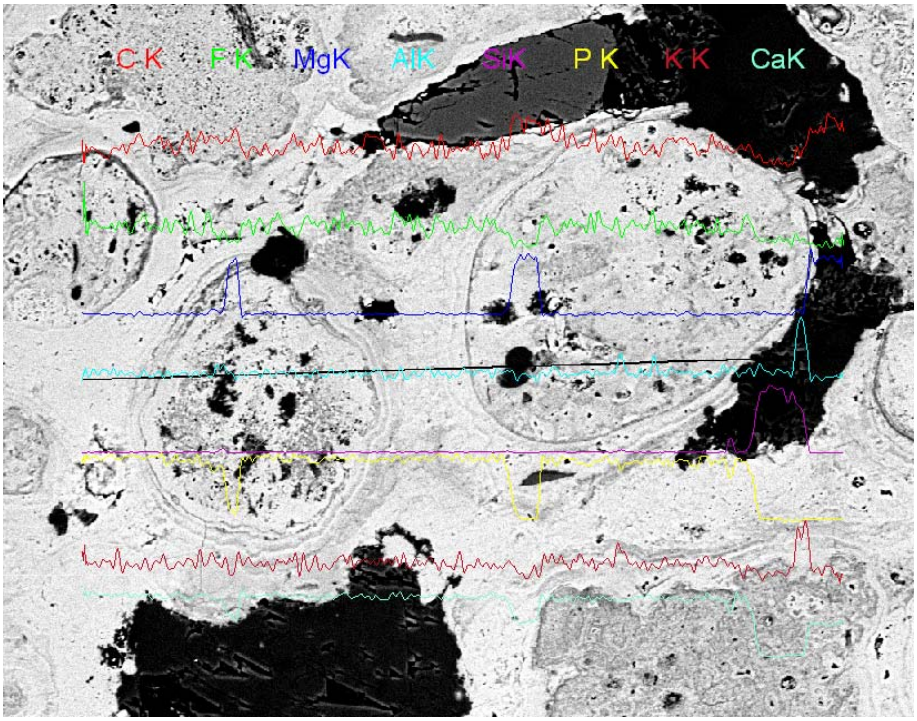

Figure DR7. Elemental line scanning of thin sections from typical coated phosphatic grains (reworked phosphorite) in the Gezhongwu section.

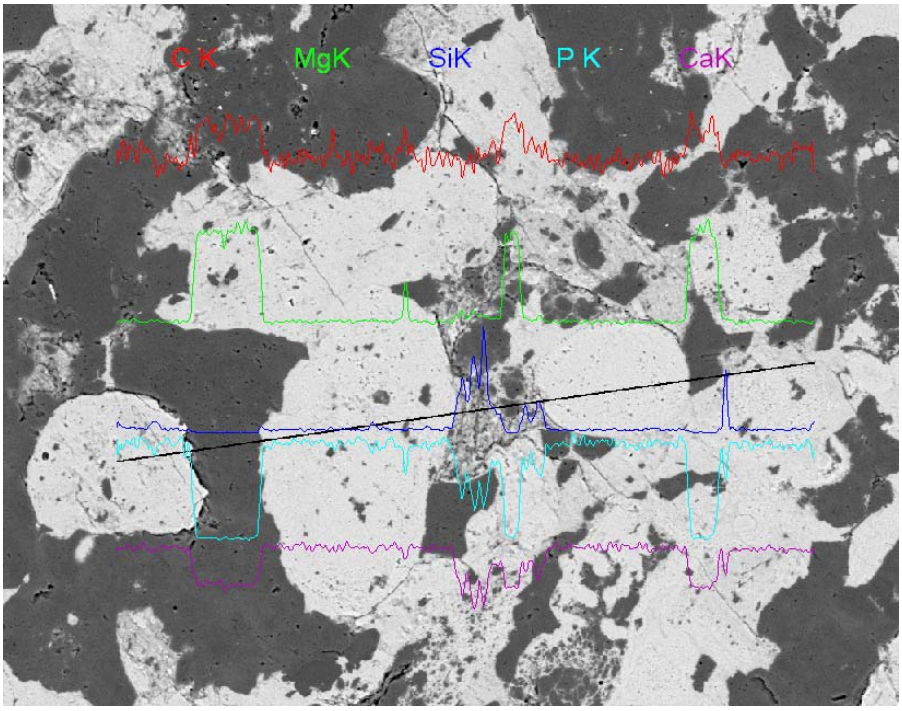

Figure DR8. Elemental line scanning of thin sections from typical pristine phosphorite in the Gezhongwu section.

References for Data Repository Items

Carignan J. and Wen H.J., 2007, Scaling NIST SRM 3149 for Se isotope analysis and isotopic variations of natural samples, Chemical Geology: v. 242, p. 347–350.

Guo, Q., Shields, G.A., Liu, C., Strauss, H., Zhu, M., Pi, D., Goldberg, T., Yang, X., 2007, Trace element chemostratigraphy of two Ediacaran-Cambrian successions in South China: Implications for organosedimentary metal enrichment and silicification in the Early Cambrian: Palaeogeography, Palaeoclimatology, Palaeoecology, v. 254, p. 194-216.

Jiang, S.Y., Pi, D.H., Heubeck, C., Frimmel, H., Liu, Y.P., Deng, H.L., Ling, H.F., and Yang, J.H., 2009, Early Cambrian ocean anoxia in South China: Nature, p. 459, p. E5-E6.

Pietruszka, A.J., Walker, R.J. and Candela, P.A., 2006, Determination of mass-dependent molybdenum isotopic variations by MC-ICP-MS: An evaluation of matrix effects, Chemical Geology: 225, p. 121-136.

Poulson, R.L., Siebert, C., McManus J., and Berelson, W.M., 2006, Authigenic molybdenum isotope signatures in marine sediments, Geology: v. 34, p. 617-620.

Sawaki, Y., Nishizawa, M., Suo, T., Komiya, T., Hirata, T., Takahata, N., Sano, Y., Han, J., Kon, Y., and Maruyama, S., 2008, Internal structures and U-Pb ages of zircons from a tuff layer in the Meishucunian Formation, Yunnan Province, South China: Gondwana Research, v. 14, p. 148–158.

Steiner, M., Wallis, E., Erdtmann, B., Zhao, Y.L., Yang, R.D., 2001, Submarine-hydrothermal exhalative ore layers in black shales from South China and associated fossils -- insights into a Lower Cambrian facies and bio-evolution: Palaeogeography, Palaeoclimatology, Palaeoecology, v. 169, p. 165-191.

Wen H.J., Carignan, J., Cloquet, C., Zhu, X.K., and Zhang, Y.X., 2010, Isotopic delta values of molybdenum standard reference and prepared solutions measured by MC-ICP-MS: Proposition for delta zero and secondary references: Journal of Analytical Atomic Spectrometry, v. 25, p. 716-721.

Zhang, Y.X., Wen, H.J., Fan, H.F., 2009, Chemical pretreatment methods for measurement of Mo isotope ratio on geological samples: Chinese Journal of Analytical Chemistry, v. 37, p. 216-220.

Zhu, R.X., Li, X.H., Hou, X.G., Pan, Y.X., Wang, F., Deng, C.L., and He, H.Y., 2009, SIMS U-Pb zircon age of a tuff layer in the Meishucun section, Yunnan, southwest China: Constraint on the age of the Precambrian-Cambrian boundary: Science in China Series D: Earth Sciences, v. 52, p. 1385-1392.

Zhu, X.K., O'Nions, R.K., Guo, Y., Belshax, N.S., and Rickard, D., 2000, Determination of natural Cu-isotope variations by plasma-source mass spectrometry: implications for use as geochemical tracers, Chemical Geology: v. 163, p. 139–149.